INTERNATIONAL JOURNAL FOR NUMERICAL METHODS IN ENGINEERING
Int. J. Numer. Meth. Engng. **45**, 503–528 (1999)

FINITE ELEMENT SOLUTION OF FREE-SURFACE SHIP-WAVE PROBLEMS

SERGIO R. IDELSOHN[†], EUGENIO OÑATE[*] AND CARLOS SACCO

International Centre for Numerical Methods in Engineering (CIMNE), Universidad Politécnica de Cataluña, Edificio C1, Gran Capitán s/n, 08034 Barcelona, Spain

SUMMARY

An unstructured finite element solver to evaluate the ship-wave problem is presented. The scheme uses a non-structured finite element algorithm for the Euler or Navier–Stokes flow as for the free-surface boundary problem. The incompressible flow equations are solved via a fractional step method whereas the non-linear free-surface equation is solved via a reference surface which allows fixed and moving meshes. A new non-structured stabilized approximation is used to eliminate spurious numerical oscillations of the free surface. Copyright © 1999 John Wiley & Sons, Ltd.

KEY WORDS: free surface flows; unstructured meshes; finite elements; CFD; wave drag

1. INTRODUCTION

A ship is subject to forces of various kinds. The resistance at a desired speed determines the required engine power and thereby the fuel consumption. Minimization of the resistance is an important issue in ship design. Further, excitation of a wave pattern produced by the ship not only induces wave resistance, but may also introduce speed limitations in the vicinity of the shores for environmental reasons which must also be taken into account in ship design.

The usual simplification in ship hydrodynamic design is to separately consider the performance of the ship in still water and its behaviour in open sea. Hydrodynamic optimization of a hull primarily requires the calculation of the resistance in a calm sea and the open sea effects are generally taken into account as a wave-added resistance.

The resistance of a ship in still water can be considered as the sum of several contributions: a viscous resistance associated with the generation of boundary layers, the wave resistance, the air resistance on the superstructure and the induced resistance related to the generation of lift forces.

Wave resistance in practical cases amounts to 10–60 per cent of the total resistance of a ship in still water [1]. It increases very rapidly at high speeds dominating the viscous component for fast displacement ships. Furthermore, wave resistance is very sensitive to the hull form design and

[*] Correspondence to: Eugenio Oñate, International Centre for Numerical Methods in Engineering (CIMNE), Universidad Politécnica de Cataluña, Edificio C1, Campus Norte UPC, Gran Capitán s/n, 08034 Barcelona, Spain. E-mail: onate@etseccpb.upc.es
[†] Professor at Universidad Nacional del Litoral, Santa Fe, Argentina. Visiting Professor at CIMNE

CCC 0029–5981/99/170503–29$17.50

Received 15 October 1997
Revised 2 July 1998

easily affected by small shape modifications. For all these reasons, the possibility to predict and reduce the wave resistance is an important target.

The prediction of a wave pattern and wave resistance of a ship has challenged mathematicians and hydrodynamicists for over a century. The Boundary Element Method (BEM) forms the basis of the majority of the computational algorithms developed in recent years. Here the flow problem is solved using a simple potential model. BEM methods, known by hydrodynamicists as Panel Methods may be classified into two categories. The first one uses the Kelvin wave source as the elementary singularity. The main advantage of such scheme is the automatic satisfaction of the radiation condition. The theoretical background of this method was reviewed by Wehausen [2], while computational aspects can be found in the literature and in a series of Wave Resistance Workshops [3, 4]. The second class of BEM schemes uses the Rankine source as the elementary singularity. This procedure was first presented by Dawson [5]. Since then it has been applied widely as a practical method and many improvements have been made to account for the non-linear wave effects. Among these a succesful example is the Rankine Panel Method [6–15]. The Finite Element Method (FEM) has also been occasionally used to solve the free-surface potential flow problem in two- and three-dimensional domains [16, 17].

In recent years, the advent of advanced numerical schemes for the Euler and Navier–Stokes equations has enabled a more realistic prediction of wave resistance problems. The incompressible three-dimensional flow equations have been solved mainly with two main type solvers. The first class is based on projection schemes [18–24]. A velocity field is predicted in a first step. Conservation of mass is enforced in a second step by solving a Poisson equation yielding a new pressure field. Finally, the velocities are updated using the new pressures. The second class of methods is based on introducing a pseudo-compressible flow and using algorithms developed for this kind of problems. Typical examples are artificial compressibility schemes [25–30] in which the infinite speed of sound is reduced to a finite number by adding a time derivative to the divergence equation, or the use of preconditioning matrices [31, 32]. In this paper, we have chosen a semi-explicit projection method where the velocity solution steps are solved explicitly and the pressure evaluation involves the implicit solution of a simple Poisson equation. Also as the pressure is specified over a considerable portion of the domain, the use of an iterative symmetric solver provides very fast convergence of the implicit step.

Independent of the flow equation used, the free-surface boundary condition has been solved in different manners. The exact free surface condition is non-linear and several linearizations have been proposed [33–39]. Some of them use a fixed domain and others a moving one. In this paper, the full non-linear free-surface equation is used but it is applied on a reference surface not necessarily coinciding with the free-surface itself. In this way the updating of the surface mesh is minimized and sometimes not even necessary.

Finally, the solution of the free-surface equation in a bounded domain imposes the necessity of a radiation condition to eliminate spurious waves. The most classical way to introduce this condition was proposed by Dawson [5] who used a four upwind point formula to evaluate the first derivatives appearing in the free-surface equation. This is probably the main reason why the large majority of codes predicting the wave resistance of ships uses structured meshes. Other authors introduce a fourth-order derivative on the free-surface equation, without a clear explanation of the reasons [27, 40]. In this paper, the free-surface equation is treated as a pure convection equation and it is stabilized using a consistent procedure. This approach allows better to understand the mathematical reasons of introducing higher-order derivative terms. In addition, it also allows to solve the radiation condition with non-structured meshes.

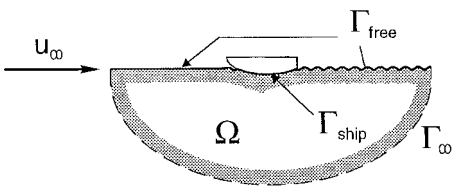

Figure 1. Ship-like body with constant forward velocity in an infinitely deep and calm sea

In the last part of the paper some examples of application of the approach proposed to the hydrodynamic analysis of a submerged NACA profile, a Wigley hull, a fast ferry and a racing sail boat are presented.

2. THE NON-LINEAR FREE-SURFACE EQUATIONS

Figure 1 shows the reference co-ordinate system used in this work. The ship hull pierces the uniform flow and is held fixed inplace. The mathematical solution to this problem consists of finding a flow solution in all the domain Ω, satisfying particular boundary conditions. Let

$$F(\vec{\mathbf{u}}, p, \rho, \mu) = 0 \quad \text{on } \Omega \tag{1}$$

represent a non-linear set of equations to be satisfied on the fluid domain Ω, where $\vec{\mathbf{u}}$ denotes the velocity vector, with components u, v and w, p is the pressure, ρ the density and μ the fluid viscosity. Equation (1) may represent the laminar or turbulent Navier–Stokes equations, the Euler equations or the simpler potential flow equations.

The boundary conditions of this problem are the classical ones in fluid flow with exception of the free-surface condition which is the only one to be described in detail here.

When the effects of surface tension are neglected, the boundary conditions on the free surface consist of two equations: the dynamic condition stating that the pressure distribution on the surface is known, and the kinematic condition stating that the free-surface is a material one. Mathematically, these two boundary conditions may be expressed as

$$p = \bar{p} \tag{2}$$

$$u_n = \mathbf{n}^{\mathrm{T}} \vec{\mathbf{u}} = 0 \quad \text{on } \Gamma_{\mathrm{f}} \tag{3}$$

where u_n is the component of the velocity in the normal direction to the free-surface Γ_{f}, $\mathbf{n} = [l, m, n]^{\mathrm{T}}$ is the unit vector normal to the free-surface and $\bar{p}$ is a known pressure field, usually considered to be the constant atmospheric pressure.

For non-breaking waves, the free-surface boundary condition may be written as a function of a two-dimensional variable $\beta(x, y)$ representing the free-surface equation as

$$z = \beta(x, y) \tag{4a}$$

$$u\frac{\partial \beta}{\partial x} + v\frac{\partial \beta}{\partial y} - w = 0 \quad \text{on } \Gamma_{\mathrm{f}} \tag{4b}$$

For simplicity we will write (4b) as

$$w = \mathbf{u}^{\mathrm{T}} \boldsymbol{\nabla} \beta \quad \text{on } z = \beta \tag{5a}$$

with

$$\mathbf{u}^{\mathrm{T}} = [u, v] \quad \text{and} \quad \boldsymbol{\nabla}^{\mathrm{T}} = \left[\frac{\partial}{\partial x}, \frac{\partial}{\partial y} \right] \tag{5b}$$

For non-stationary problems, equation (5) becomes

$$\frac{D\beta}{Dt} = w = \frac{\partial \beta}{\partial t} + \mathbf{u}^{\mathrm{T}} \nabla \beta \quad \text{on } z = \beta \tag{6}$$

Equations (5) or (6) represent a non-linear boundary condition of the unknowns $\mathbf{u}$ and β, prescribed on an unknown free boundary (i.e. on $z = \beta$).

Let us assume that the viscosity effects are negligible in the vicinity of the free-surface. Under this assumption, Bernoulli equation may be used near the free-surface, i.e.

$$\frac{\bar{p}}{\rho} + \frac{1}{2} |\vec{\mathbf{u}}|^2 + g\beta = \mathrm{C} \tag{7}$$

where C is a constant value. From equation (7)

$$\beta = \frac{1}{g} \left[C - \frac{1}{2} |\vec{\mathbf{u}}|^2 - \frac{\bar{p}}{\rho} \right] \tag{8}$$

and substituting equation (8) into (5) gives

$$2gw + \mathbf{u}^{\mathrm{T}} \boldsymbol{\nabla} |\vec{\mathbf{u}}|^2 = -2\mathbf{u}^{\mathrm{T}} \nabla \frac{\bar{p}}{\rho} \quad \text{on } z = \beta \tag{9}$$

Equation (9) shows clearly the two types of non-linearities involved in the free-surface problem: (1) the term $\mathbf{u}^{\mathrm{T}} \nabla |\vec{\mathbf{u}}|^2$, including third-order velocities, and (2) the unknown position of the free-surface itself. Both non-linearities must be jointly solved using a linearized iterative algorithm. The first non-linearity can be interpreted as a classical non-linear problem, whereas the second one is a standard free boundary problem.

The free boundary problem is directly related to the updating of the finite element mesh which usually is a costly process introducing contact problems and mesh distortion. For this reason, in this paper, the free-surface will be written as a function of a reference surface. This allows to reduce, and sometimes, to eliminate the mesh updating process, thus improving considerably the computational efficiency of the iterative algorithm.

3. ITERATIVE METHODS FOR SOLVING THE FREE-SURFACE PROBLEM

3.1. Bernoulli method

In the past years, many algorithms to solve the free-surface equations have been proposed. The simplest one is to start with an initial value of the free-surface position $\beta = \beta_0$ (normally the non-wave solution). This allows to evaluate the velocity field $\vec{\mathbf{u}}_o$ and then, using (8), to estimate

a new β_1 position. This can be used to update the mesh and so on. The method is equivalent to solve (9) using the last iteration solution to evaluate $|\vec{\mathbf{u}}|$, i.e.

$$2gw_i + \mathbf{u}_i^{\mathrm{T}} \boldsymbol{\nabla} \left(|\vec{\mathbf{u}}_{i-1}|^2 + \frac{\bar{p}}{\rho} \right) = 0 \quad \text{on } z = \beta_{i-1} \tag{10}$$

This method has a very limited rate of convergence.

3.2. Pseudo-concentration method

An interesting method to solve the non-linear free-surface problem, is the so-called volume of fluid or pseudo-concentration method. This technique is extensively used for the tracking of fluid fronts in mould-filling problems [41]. The method consists in transporting within a fixed volume a pseudo-concentration function β such that $\partial\beta/\partial z = -1$. The transport equation equivalent to (5) reads

$$\vec{\mathbf{u}}^{\mathrm{T}} \vec{\boldsymbol{\nabla}} \beta = 0 \tag{11}$$

where

$$\vec{\mathbf{u}}^{\mathrm{T}} = [u, v, w] \quad \text{and} \quad \vec{\boldsymbol{\nabla}}^{\mathrm{T}} = \left[\frac{\partial}{\partial x}, \frac{\partial}{\partial y}, \frac{\partial}{\partial z} \right] \tag{12}$$

Equation (11) is now solved at each iteration using the value of $\vec{\mathbf{u}}$ provided by the flow solver. This algorithm reads

$$-w_{i-1} + \mathbf{u}_{i-1}^{\mathrm{T}} \nabla \beta_i = 0 \quad \text{on } z = \beta_{i-1} \tag{13}$$

Equation (13) is typically solved numerically using a discretization of the wave height β different from that chosen for the velocity field.

3.3. Transpiration method

An improved version of the pseudoconcentration technique is to replace w_{i-1} by w_i in the first term of equation (13). This gives

$$-w_i + \mathbf{u}_{i-1}^{\mathrm{T}} \nabla \beta_i = 0 \quad \text{on } z = \beta_{i-1} \tag{14}$$

The name of transpiration method emerges from the fact that the normal velocity to the free surface w_i is introduced as an external unknown flow. This method will be detailed in the next section and it will be used in all the examples shown in this paper.

In order to better understand the three methods described above, they can be written in a compact way as

(1) Bernoulli method: $\mathbf{u}_i^{\mathrm{T}} \boldsymbol{\nabla} \beta_{i-1} - w_i = 0$ on $z = \beta_{i-1}$.
(2) Pseudo-concentration method: $\mathbf{u}_{i-1}^{\mathrm{T}} \nabla \beta_i - w_{i-1} = 0$ on $z = \beta_{i-1}$.
(3) Transpiration method: $\mathbf{u}_{i-1}^{\mathrm{T}} \boldsymbol{\nabla} \beta_i - w_i = 0$ on $z = \beta_{i-1}$.

Bernoulli method does not converge very well while the transpiration method shows the better convergence rates.

All these three methods iterate using the previous evaluation of the free surface (β_{i-1}) as a new boundary condition. The new discretized domain may be obtained by remeshing. This is not very efficient from the computational point of view as remeshing is indeed an expensive step in three-dimensional CFD problems.

In this paper the transpiration method is used, but the non-linearities due to the free-surface equation itself are treated separately from those arising from the free-surface position. This will be defined from a *reference surface* by means of a Taylor series. In this way, the free-surface boundary may move while the reference surface remains fixed.

4. FREE-SURFACE REFERENCE ITERATIONS

There are several variations of the transpiration iterative scheme. The simplest one, the so-called *linearized wave theory*, evaluates w_i on $z=0$ and then uses a perturbation technique to linearize the term $\nabla\beta_i$. For instance, using equation (8) gives after linearizing,

$$\nabla\beta_i = -\frac{1}{2g}\nabla|\vec{\mathbf{u}}_i|^2 = -\frac{1}{g}\vec{\mathbf{u}}_0^{\mathrm{T}}\nabla\vec{\mathbf{u}}_i \tag{15}$$

Equation (14) then becomes linear in $\vec{\mathbf{u}}$. The different linearized theories depend on the choice of the velocity of the reference flow. In particular, the thin ship linearized theory uses: $\vec{\mathbf{u}}_0 = \text{constant}$ while the so-called Dawson theory [5] uses for $\vec{\mathbf{u}}_0$ the flow field obtained from the wave-free solution. Many other linearized theories have been proposed [1]. In most cases, the free boundary is fixed and only one iteration is needed to obtain the results. Probably for this reason, fixed mesh techniques have been mainly related to linearized theories. We will describe next a procedure in which the mesh may remain fixed but the free boundary may move during a non-linear iterative algorithm.

The error in all linear theories derives from the application of the boundary condition on $z=\beta_{i-1}$ and not on $z=\beta$.

In order to improve this approximation, the velocity $\vec{\mathbf{u}}|_{z=\beta}$ may be expanded in a Taylor series in the z direction from a β_{ref} reference position, i.e.

$$\vec{\mathbf{u}}|_{z=\beta} = \vec{\mathbf{u}}|_{z=\beta_{\mathrm{ref}}} + \frac{\partial\vec{\mathbf{u}}}{\partial z}(\beta-\beta_{\mathrm{ref}}) + 0(\beta-\beta_{\mathrm{ref}})^2 \tag{16}$$

Substituting equation (16) into (5) gives

$$w + \frac{\partial w}{\partial z}(\beta-\beta_{\mathrm{ref}}) = \left(u + \frac{\partial u}{\partial z}(\beta-\beta_{\mathrm{ref}})\right)\frac{\partial\beta}{\partial x} + \left(v + \frac{\partial v}{\partial z}(\beta-\beta_{\mathrm{ref}})\right)\frac{\partial\beta}{\partial y} \tag{17}$$

Neglecting third-order terms in equation (17) leads to

$$w = \mathbf{u}^{\mathrm{T}}\nabla\beta - \frac{\partial w}{\partial z}(\beta-\beta_{\mathrm{ref}}) \quad \text{on } z=\beta_{\mathrm{ref}} \tag{18}$$

Equation (18) applied on $z=\beta_{\mathrm{ref}}$ is still an approximation which holds for relatively small values of β, but it is a higher-order approximation than directly applying equation (5) on $z=0$. Two options are now possible: (1) to iterate on the free-surface solution while keeping the reference surface ($z=0$) fixed and changing only the free-surface β_i, or (2) the reference surface can also be updated at each iteration by $z=\beta_{i-1}$.

Taking into account the incompressibility flow condition, equation (18) may be written as

$$w = \frac{\partial}{\partial x}(u\beta) + \frac{\partial}{\partial y}(v\beta) - \left(\frac{\partial u}{\partial x} + \frac{\partial v}{\partial y}\right)\beta_{\text{ref}} = \nabla\cdot(\mathbf{u}\beta) - \nabla\cdot(\mathbf{u})\beta_{\text{ref}} \tag{19}$$

The new iterative procedure stands:

$$\nabla\cdot(\mathbf{u}_{i-1}\beta_i) - w_i = \nabla\cdot(\mathbf{u}_{i-1})\ \beta_{\text{ref}} \quad \text{on } z = \beta_{\text{ref}} \tag{20}$$

where β_{ref} is any reference surface close to the free-surface. In general, we will use $\beta_{\text{ref}} = 0$, but any other reference may be considered. In this way, the free-surface position β_i moves at each iteration until a converged solution is found, while the reference surface can remain fixed during the iterative process.

For transient problems, equation (20) becomes

$$\frac{\partial \beta_i}{\partial t} + \nabla\cdot(\mathbf{u}_{i\mu_i-1}\beta_i) - w_i = \nabla\cdot(\mathbf{u}_{i-1})\ \beta_{\text{ref}} \quad \text{on } z = \beta_{\text{ref}} \tag{21}$$

5. NUMERICAL STABILIZATION PROCEDURE

It is well known that to solve numerically an advection equation as equation (20), in which first-order derivatives are present, spurious numerical oscilations must be stabilized. A possible stabilization procedure is to add to equation (20) a numerical diffusion proportional to the second derivative of β along the flow direction. Other posibilities are to evaluate the first derivative $\partial\beta/\partial x$ in some upwind point or to use Petrov–Galerkin upwind weighting functions. Unfortunately, equations like (14) or the improved version (20) have shown to be very sensitive to the stabilization terms introduced, giving in some cases, very diffusive results, or conversely, results with spurious waves.

Several enhanced stabilization procedures have been proposed in the past to solve the free-surface equations using finite-difference or panel methods with structured grids and some are described next. A more consistent stabilization procedure applicable to non-structured finite element meshes will be presented in the next section.

5.1. Dawson upwind stabilization

For the 2-D case and taking $\beta_{\text{ref}} = 0$, equation (20) may be written in a simpler manner as

$$\frac{\partial f}{\partial x} - w = q \tag{22a}$$

with

$$f = u_{i-1}\beta_i, \quad w = w_i, \quad q = \frac{\partial u_{i-1}}{\partial x}\beta_{\text{ref}} \tag{22b}$$

Dawson [5] proposed to evaluate $\partial f/\partial x$ using a four-point upwind operator which eliminates errors from the second and fourth derivative terms but not from the third one. This is equivalent to fit through the four upwinded points the following incomplete polynomial:

$$f = a_1 + a_2 x + a_3 x^2 + a_4 x^4 \tag{23}$$

and evaluate the first derivative $\partial f/\partial x$ at point j (Figure 2).

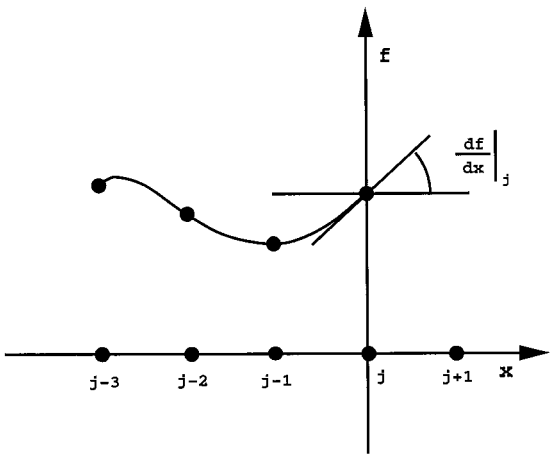

Figure 2. Reference co-ordinate for the four upwind points formula

For uniform grids, Dawson's formula reads

$$\left.\frac{\partial f}{\partial x}\right|_j = \frac{1}{6h}(10f_j - 15f_{j-1} + 6f_{j-2} - f_{j-3}) \tag{24}$$

This expression can also be extended to non-uniform grids.

Dawson's formula has been succesfully used in a large number of 2-D and 3-D problems discretized with structured grids.

5.2. *A more centred upwind stabilization*

One of the problems of Dawson's formula is the use of four upwind points. This increases considerably the bandwidth of the system to be solved and introduces some difficulties in the case of non-structured meshes. An improved version of Dawson's scheme may be obtained using the same polynomial aproximation but fitting three upwind points and one downwind point (Figure 3). For constant grids this gives

$$\left.\frac{\partial f}{\partial x}\right|_j = \frac{1}{18h}(7f_{j+1} + 6f_j - 15f_{j-1} + 2f_{j-2}). \tag{25}$$

Note that for obtaining this formula, the co-ordinate axes have been fixed on the $(j+1)$th point as indicated in Figure 3.

This formula has shown to be as accurate as the original Dawson one, but it is more centred, thus improving considerably the bandwidth of the system.

5.3. *Centred stabilization schemes: Oñate's stabilization*

For non-structured meshes, both previous schemes are difficult to use and therefore they are not suitable for a general finite element method (FEM). Standard stabilization in the FEM is typically

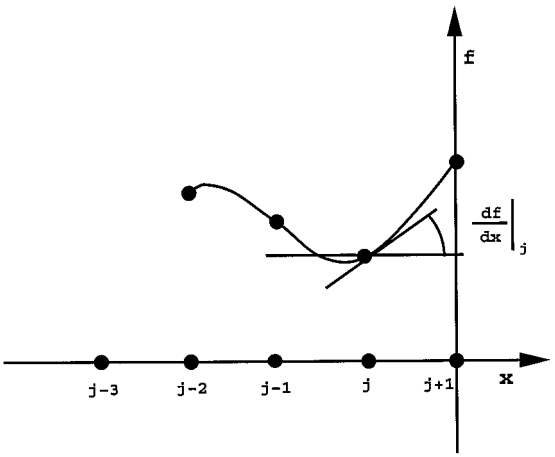

Figure 3. Refernce co-ordinates for the enhanced Dawson's formula using two-point upwind and one-point downwind

introduced by adding to equation (22) a numerical diffusion:

$$\frac{\partial f}{\partial x} - \frac{\bar{h}}{2}\frac{\partial^2 f}{\partial x^2} - w = q \tag{26}$$

where $\bar{h}$ is the upwind parameter defined as a *characteristic length*. This numerical diffusion may be mathematically justified using the Finite Increment Calculus appproach proposed by Oñate for advective–diffusive transport and fluid flow problems in [42]. The analogy of this approach with alternative stabilization methods can be found in [42–44].

Centred first and second derivatives may be obtained with a three-point centred formula as

$$\left.\overline{\frac{\partial f}{\partial x}}^{3}\right|_j = \frac{f_{j+1} - f_{j-1}}{2h}; \qquad \left.\overline{\frac{\partial^2 f}{\partial x^2}}^{3}\right|_j = \frac{f_{j+1} - 2f_j - f_{j-1}}{h^2} \tag{27}$$

Higher-order derivatives and more precise first and second derivatives, may be computed with the following five-point centred schemes:

$$\begin{aligned}
f_{j+1} &= f_j + h\frac{\partial f}{\partial x} + \frac{h^2}{2}\frac{\partial^2 f}{\partial x^2} + \frac{h^3}{6}\frac{\partial^3 f}{\partial x^3} + \frac{h^4}{24}\frac{\partial^4 f}{\partial x^4}\\
f_{j-1} &= f_j - h\frac{\partial f}{\partial x} + \frac{h^2}{2}\frac{\partial^2 f}{\partial x^2} - \frac{h^3}{6}\frac{\partial^3 f}{\partial x^3} + \frac{h^4}{24}\frac{\partial^4 f}{\partial x^4}\\
f_{j+2} &= f_j + 2h\frac{\partial f}{\partial x} + 2h^2\frac{\partial^2 f}{\partial x^2} + \frac{4}{3}h^3\frac{\partial^3 f}{\partial x^3} + \frac{2}{3}h^4\frac{\partial^4 f}{\partial x^4}\\
f_{j-2} &= f_j - 2h\frac{\partial f}{\partial x} + 2h^2\frac{\partial^2 f}{\partial x^2} - \frac{4}{3}h^3\frac{\partial^3 f}{\partial x^3} + \frac{2}{3}h^4\frac{\partial^4 f}{\partial x^4}
\end{aligned} \tag{28}$$

Then

$$\left.\overline{\frac{\partial^3 f}{\partial x^3}}^5\right|_j = \frac{1}{2h^3}(f_{j+2} - 2f_{j+1} + 2f_{j-1} - f_{j-2}) \tag{29}$$
$$\left.\overline{\frac{\partial^4 f}{\partial x^4}}^5\right|_j = \frac{1}{h^4}(f_{j+2} - 4f_{j+1} + 6f_j - 4f_{j-1} + f_{j-2})$$

and

$$\begin{aligned}\left.\overline{\frac{\partial f}{\partial x}}^5\right|_j &= \left.\overline{\frac{\partial f}{\partial x}}^3\right|_j - \frac{h^2}{6}\left.\overline{\frac{\partial^3 f}{\partial x^3}}^5\right|_j \\ \left.\overline{\frac{\partial^2 f}{\partial x^2}}^5\right|_j &= \left.\overline{\frac{\partial^2 f}{\partial x^2}}^3\right|_j - \frac{h^2}{12}\left.\overline{\frac{\partial^4 f}{\partial x^4}}^5\right|_j\end{aligned} \tag{30}$$

In the above the notation $\overline{\partial^2 f}^5/\partial x^2|_j$ denotes the second derivative of f evaluated at point j using five centred points, and so on.

Substituting equation (30) into (26) gives

$$q_j + w_j = \left.\overline{\frac{\partial f}{\partial x}}^3\right|_j - \frac{\bar{h}}{2}\left.\overline{\frac{\partial^2 f}{\partial x^2}}^3\right|_j - \frac{h^2}{2}\left.\overline{\frac{\partial^3 f}{\partial x^3}}^5\right|_j + \frac{\bar{h}h^2}{24}\left.\overline{\frac{\partial^4 f}{\partial x^4}}^5\right|_j \tag{31}$$

The main difference between standard numerical diffusion upwind schemes used in FEM and that proposed here is the accuracy in the evaluation of the first and second derivatives in equations (22) and (26). Equation (31) is in fact equivalent to (26) but taking into account the accuracy required in the evaluation of each derivative term.

The pending issue is the computation of the characteristic length parameter $\bar{h}$. The simplest choice $\bar{h} = h$, where h is the distance between two points in space, can lead to overdiffusive results in some cases. A consistent procedure for the computation of the characteristic length parameter has been proposed by Oñate et al. [42, 43].

It is interesting to note that the upwind finite-difference stabilization approach described by equation (25) is equivalent to the stabilized centred scheme represented by

$$q_j + w_j = \left.\overline{\frac{\partial f}{\partial x}}^3\right|_j - \frac{-h^2}{9}\left.\overline{\frac{\partial^3 f}{\partial x^3}}^5\right|_j + \frac{h^3}{18}\left.\overline{\frac{\partial^4 f}{\partial x^4}}^5\right|_j \tag{32}$$

In the same way it can be shown that Dawson's formula (24) is equivalent to the more precise centred scheme including the following higher-order centred derivatives:

$$q_j + w_j = \left.\overline{\frac{\partial f}{\partial x}}^3\right|_j - \frac{h^2}{3}\left.\overline{\frac{\partial^3 f}{\partial x^3}}^5\right|_j + \frac{h^4}{6}\left.\overline{\frac{\partial^5 f}{\partial x^5}}^7\right|_j - \frac{h^5}{12}\left.\overline{\frac{\partial^6 f}{\partial x^6}}^7\right|_j \tag{33}$$

All these centred schemes are easily generalized to multidimensional problems. An additional advantage is that they are suited to a weighted residual finite element context.

6. FINITE ELEMENT DISCRETIZATION OF THE FREE SURFACE

Equation (20) may be written in a local co-ordinate system (ξ, η) parallel to the flow direction $\mathbf{u}$ as

$$\frac{\partial}{\partial \xi}(|\mathbf{u}_{i-1}|\beta_i) - w_i = \frac{\partial}{\partial \xi}(|\mathbf{u}_{i-1}|)\beta_{\text{ref}} \quad \text{on } z = \beta_{\text{ref}} \tag{34}$$

where the co-ordinate ξ is parallel to the streamline flow.

Denoting, for simplicity $(|\mathbf{u}_{i-1}|\beta_i) = f$, and $(\partial/\partial\xi)(|\mathbf{u}_{i-1}|)\beta_{\text{ref}} = q$ and applying any of the stabilization schemes of previous section gives

$$\frac{\partial f}{\partial \xi} + \alpha_1 \frac{\partial^2 f}{\partial \xi^2} + \cdots = q + w_i \tag{35}$$

where α_i is the stabilization coefficient deduced from equations (31)–(33).

A weighting residual approximation to equation (35) reads

$$\int_{\beta_{\text{ref}}} W \left[\left(\frac{\partial f}{\partial \xi} + \alpha_1 \frac{\partial^2 f}{\partial \xi^2} + \cdots \right) - w_i - q \right] \mathrm{d}\Gamma = 0 \tag{36}$$

Integrating by parts the innerbracket term gives

$$\int_{\beta_{\text{ref}}} \left[\frac{\partial W}{\partial \xi} \left(f + \alpha_1 \frac{\partial f}{\partial \xi} + \cdots \right) + W(w_i + q) \right] \mathrm{d}\Gamma - \int_{S_0} Wl \left(f + \alpha_1 \frac{\partial f}{\partial \xi} + \cdots \right) \mathrm{d}S_0 = 0 \tag{37}$$

where S_0 is the 2-D boundary of the free-surface which is composed of two parts: the intersection between the ship and the free-surface and the intersection between the far away surface and the free-surface, l is the cosine of the angle between the normal to S_0 and the flow direction. This angle is 90° in the majority of the ship boundary where the ship geometry is coinciding with the streamlines. Nevertheless, in some parts, the last integral of (37) must not be neglected. On the far away free-surface boundary, the simplest way to neglect this last integral is to force β to be zero by adding a damping term in equation (34) in regions near this boundary [45].

In a FEM context, the unknown functions are approximated by

$$f = \mathbf{N}^{\mathrm{T}}\mathbf{f} \tag{38}$$

where N_j are local supported shape functions and f_j are the values of the unknown at node j.

Galerkin weighting functions $W_j = N_j$ will be used in equation (37).

The evaluation of the higher-order derivatives is performed using the same interpolations chosen for unknown fields. For instance, the term

$$\int_{\beta_{\text{ref}}} \frac{\partial W}{\partial \xi} \alpha_2 \frac{\partial^2 f}{\partial \xi^2} \mathrm{d}\Gamma$$

is solved by approximating the second derivatives as

$$\frac{\partial^2 f}{\partial \xi^2} = \mathbf{N}^{\mathrm{T}}\mathbf{f}'' \tag{39}$$

where $f_j'' = (\partial^2 f/\partial \xi^2)_j$ is the local value of the second derivative at node j. This is computed by

$$f_j'' \cong \frac{1}{A_j}\int_{\beta_{\text{ref}}} N_j \frac{\partial^2 f}{\partial \xi^2}\,\mathrm{d}\Gamma = \frac{1}{A_j}\left[-\int_{\beta_{\text{ref}}} \frac{\partial N_j}{\partial \xi}\frac{\partial f}{\partial \xi} + \int_{S_0} N_j l \frac{\partial f}{\partial \xi}\,\mathrm{d}S_0\right]$$

$$= \frac{1}{A_j}\left[-\int_{\beta_{\text{ref}}} \left(\frac{\partial N_j}{\partial \xi}\frac{\partial \mathbf{N}^{\mathrm{T}}}{\partial \xi}\right)\mathrm{d}\Gamma + \int_{S_0} N_j l \frac{\partial \mathbf{N}^{\mathrm{T}}}{\partial \xi}\,\mathrm{d}S_0\right]\mathbf{f} \tag{40}$$

where

$$A_j = \int_{\beta_{\text{ref}}} N_j\,\mathrm{d}\Gamma \tag{41}$$

The integrals over S_0 are computed using an identical procedure to that used for the analogous integral in equation (37).

7. ITERATIVE SOLUTION

The Euler or Navier–Stokes equations are solved using a semi-explicit Fractional Step Method (FSM) [46, 47]. This has proved to be a very suitable approach to introduce easily the free-wave condition (37). A complete solution over a time increment consists of three steps:

(a) Explicit advection prediction of the $\vec{\mathbf{u}}$ velocity from the momentum equation skipping pressure terms, i.e.

$$\vec{\mathbf{u}}^* = \vec{\mathbf{u}}_{i-1} - \Delta t[\vec{\mathbf{u}}\cdot\nabla\vec{\mathbf{u}} - \nabla\mathbf{F}_\mu]_{i-1} + ST \tag{42}$$

where $\mathbf{F}_\mu$ represents the viscosity flux and ST represents the stabilizing term typically used in fluid mechanics (e.g. SUPG, Taylor–Galerkin, Characteristic-Galerkin or others [46–48]). This step is performed explicitly.

(b) A pressure correction, to obtain the new pressure field p_i. Combining the incompressible equation

$$\nabla\cdot\vec{\mathbf{u}}_i = 0 \tag{43a}$$

with the momentum equation for the pressure

$$(\vec{\mathbf{u}}_i - \vec{\mathbf{u}}^*)\frac{1}{\Delta t} + \nabla p_i = 0 \tag{43b}$$

results in

$$\nabla^2 p_i = \frac{1}{\Delta t}\nabla\cdot\vec{\mathbf{u}}^* \tag{43c}$$

Note that this is an implicit step, but only involving the pressure unknown. Equation (43c) leads to a standard symmetric equation system which can be efficiently solved iteratively using conjugate gradient techniques.

(c) Explicit velocity correction to obtain the final velocity field $\mathbf{u}_i$,

$$\vec{\mathbf{u}}_i = \vec{\mathbf{u}}^* - \Delta t \nabla p_i \tag{44}$$

A detailed description of the FSM for the Navier–Stokes can be found in [26].

In case of steady flows the process (a)–(c) is repeated until a steady-state solution is found. Local time stepping can be used in this case to speed up the convergence [46, 47].

The free-surface boundary condition (34) or its weighting residual approximation (37) is easily introduced by taking into account the explicit (centred) time integration chosen:

$$\frac{\beta_{i+1} - \beta_i}{\Delta t^*} = -\frac{\partial}{\partial \xi}(|\vec{\mathbf{u}}|\beta_i) + w_i + q \tag{45}$$

where Δt^* is a time step not necessarily equal to the time step used for integrating the flow equations in equations (42)–(44).

The first term of the r.h.s. of equation (45) is evaluated using any of the stabilized centred schemes described previously.

After each flow iteration, the new position of the free-surface β is evaluated and this is introduced in the next iteration as a prescribed pressure at the reference free-surface in step (b). From Bernouilli equation

$$\frac{\bar{p}}{\rho} + g\beta_{i+1} = \frac{p_{\text{ref}}}{\rho} + g\beta_{\text{ref}} \tag{46a}$$

then

$$p_{\text{ref}} = \bar{p} + \rho g(\beta_{i+1} - \beta_{\text{ref}}) \tag{46b}$$

where p_{ref} represents the pressure to be introduced as a Dirichlet boundary condition on the reference free-surface at β_{ref} in equation (43c).

8. NUMERICAL RESULTS

8.1. Submerged NACA0012 profile

The first example considered is a 2-D submerged NACA0012 profile at $\alpha = 5^\circ$ angle of attack. This configuration was tested experimentally by Duncan [49] for high Reynolds numbers (Re = 400 000) and modelled numerically using the Euler equations by several authors [27, 40]. The submerged depth of the aerofoil is equal to the chord and this was used as the lenght (L) for normalizing the problem. The Froude number for all the cases tested was set to $Fr = u/\sqrt{gL} = 0{\cdot}5672$ where u is the incoming flow velocity at infinity.

This problem was run with the proposed methodology using Euler and Navier–Stokes equations. Figure 4 shows the mesh used for the Euler equations with a total of 10 149 linear triangles. Plate 1 shows the stationary free surface and the pressure distribution in the domain. The non-dimensional wave heights compare reasonably well with the experimental results of [49] represented in Figure 5(a). The convergence history for the inviscid drag force up to 60 000 iterations is plotted in Figure 5(b).

In order to compare the different stabilization schemes described in Section 5 this example was tested with both Dawson's and Oñate's formulae using different characteristic length parameters

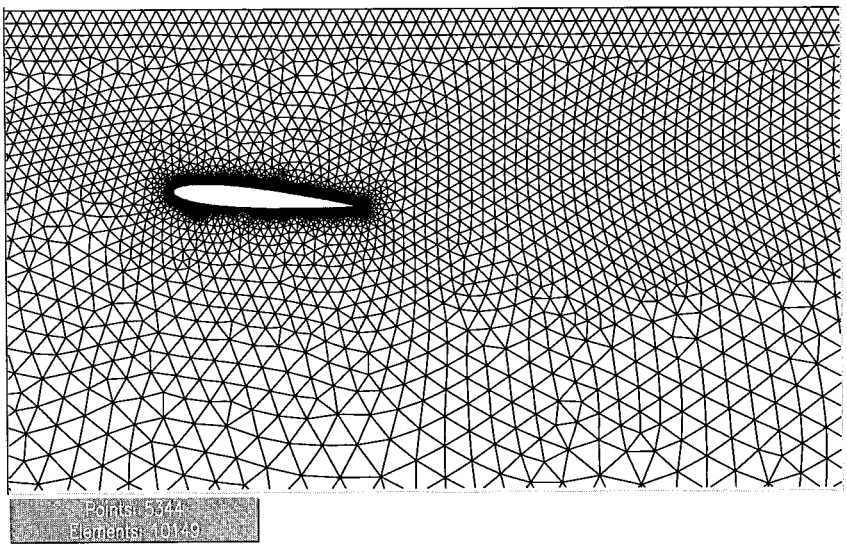

Figure 4. Submerged NACA0012. Mesh for the Euler solution

given by $\overline{h} = \alpha h$. Figure 6 shows the elevation and frequency of the waves for the different formulae. It can be seen that all the results are in good agreement with the experimental values. Best results are obtained with a low value of the $\overline{h}$ parameter equal to $\frac{1}{15}h$ where h is the length of the element laying on the free-surface.

Figure 7 shows the mesh used for the Navier–Stokes equation with a total of 35 557 triangular elements. No-slip condition were imposed on the aerofoil. With the same Froude number in the previous inviscid case, several Reynolds numbers of 500, 1000, 2000, 5000 and 10 000 were investigated.

Figure 8 shows the wave profiles for different Reynolds numbers. The upstream wave decreases as the Reynolds number increases. For $Re = 2000$ the results were similar to those reported in [49]. Unfortunately, no experimental data are available for low Re to compare the results.

Another interesting feature of this example is that if the Reynolds number exceeds a critical value, the solution does not converge to a stationary value. Figure 9(a)–9(d) shows the convergence history of the drag coefficient for Re between 500 and 10 000. Note that as the Reynolds number is increased up to 5000 the solution converges to an oscilatory solution. This behaviour is explained by the presence of vortex shedding. Plate 2(a)–2(d) show the velocity modulus contours for the different Reynolds numbers analized. The vortex shedding effect is very clear for higher Reynolds numbers (Plate 2(c) and 2(d)).

Finally, the effect of vortex shedding on the free-surface is plotted in Figure 10. The non-stationary fluid flow solution affects directly the wave problem yielding a non-stationary solution. In Figure 10 the wave elevations at different time steps for a complete cycle of the vortex shedding are represented.

In all cases, the Δt used was the critical time step of the fractional step algorithm chosen [26]. Also $\Delta t^* = \Delta t$ was chosen for the free-surface equation. The reference surface β_{ref} used was fixed to $z = 0$ (the original planar surface) and all the calculations were performed on the same fixed mesh.

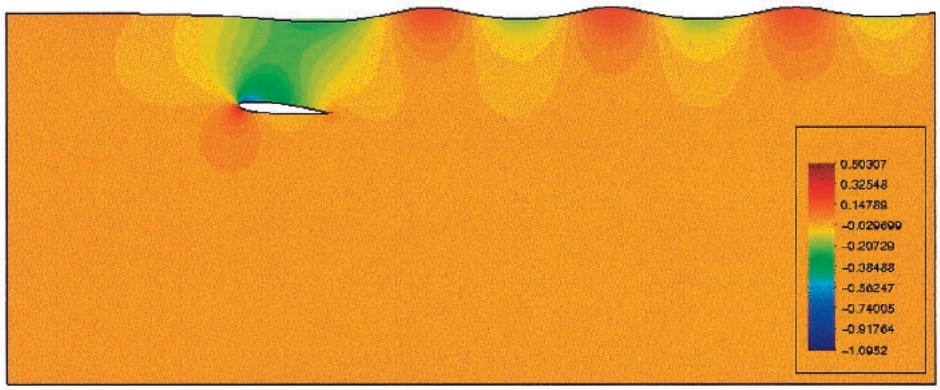

Plate 1. Submerged NACA0012. Surface elevation and pressure contours

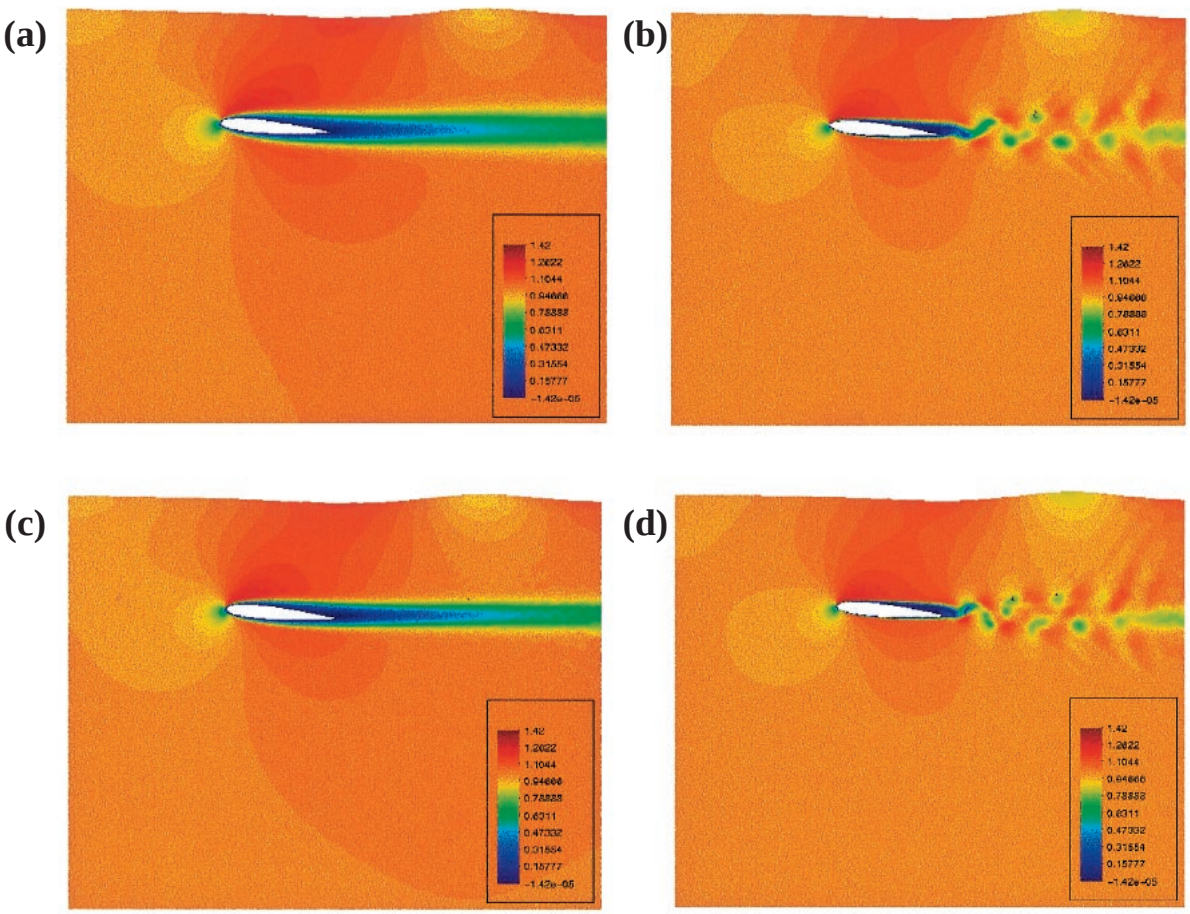

Plate 2. Submerged NACA0012. Velocity modulus contours: (a) *Re*=500; (b) *Re*=1000; (c) *Re*=5000; (d) *Re*=10 000

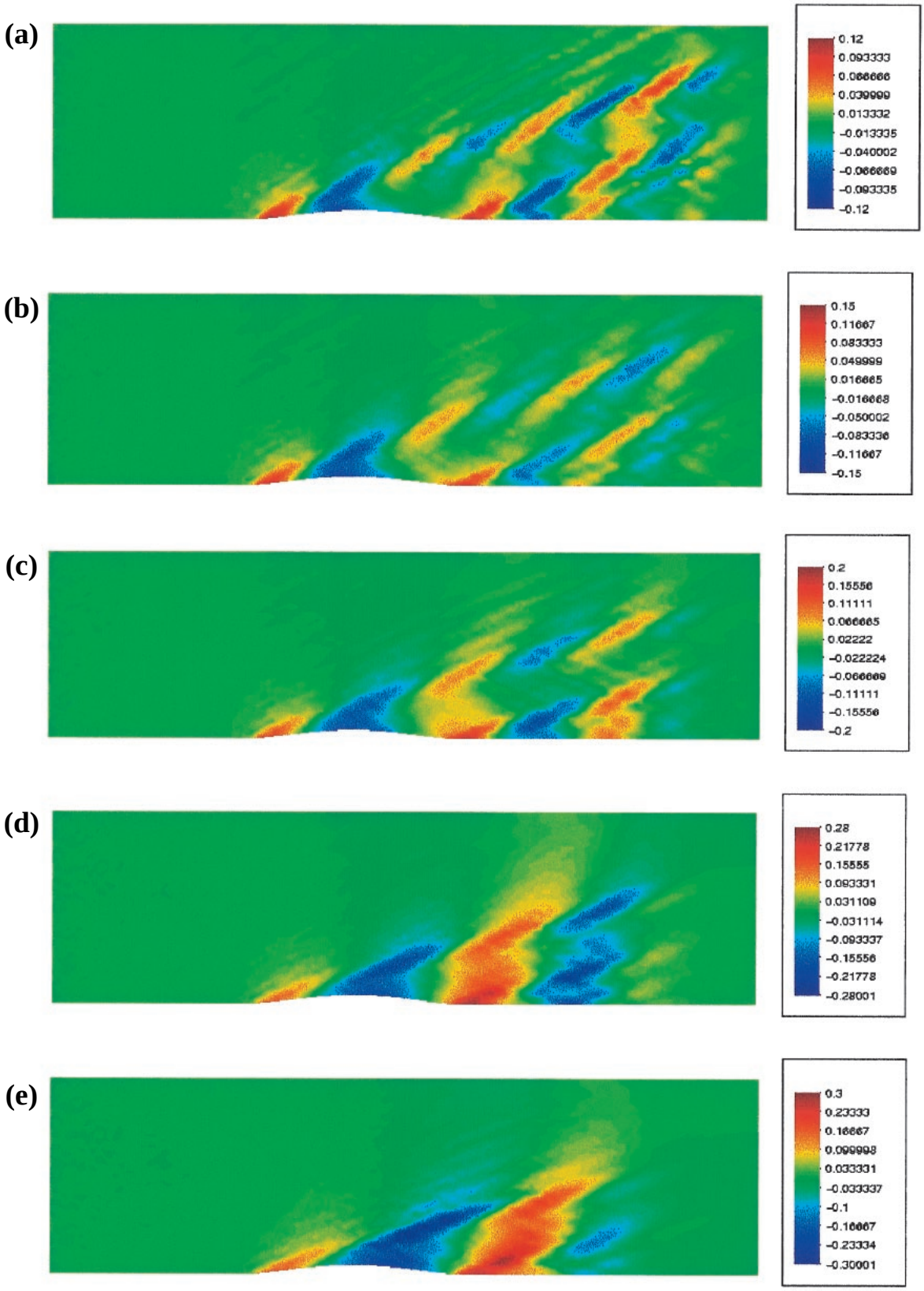

Plate 3. Wigley hull. Wave pattern elevation: (a) *Fr*=0·30; (b) *Fr*=0·325; (c) *Fr*=0·35; (d) *Fr*=0·40; (e) *Fr*=0·45

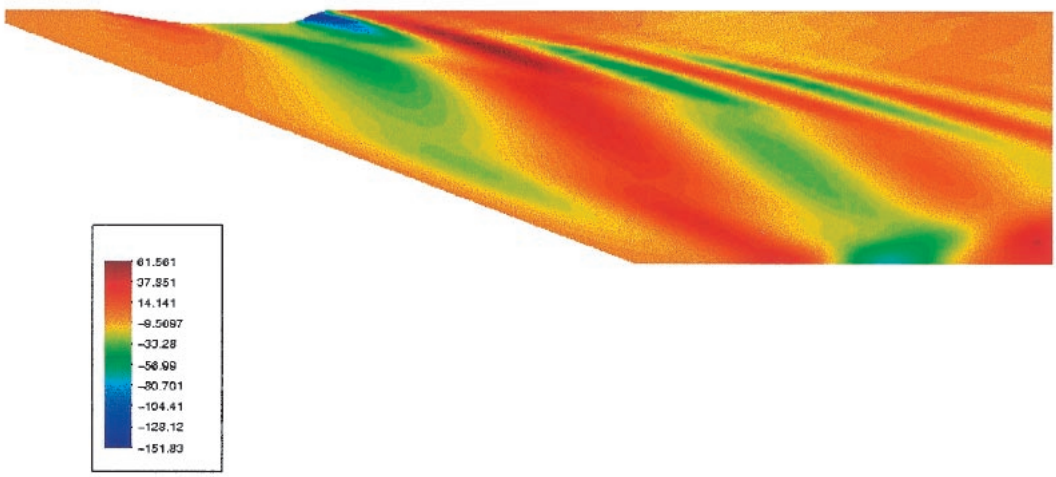

Plate 4. Fast ferry hull. Wave pattern at 40 knots

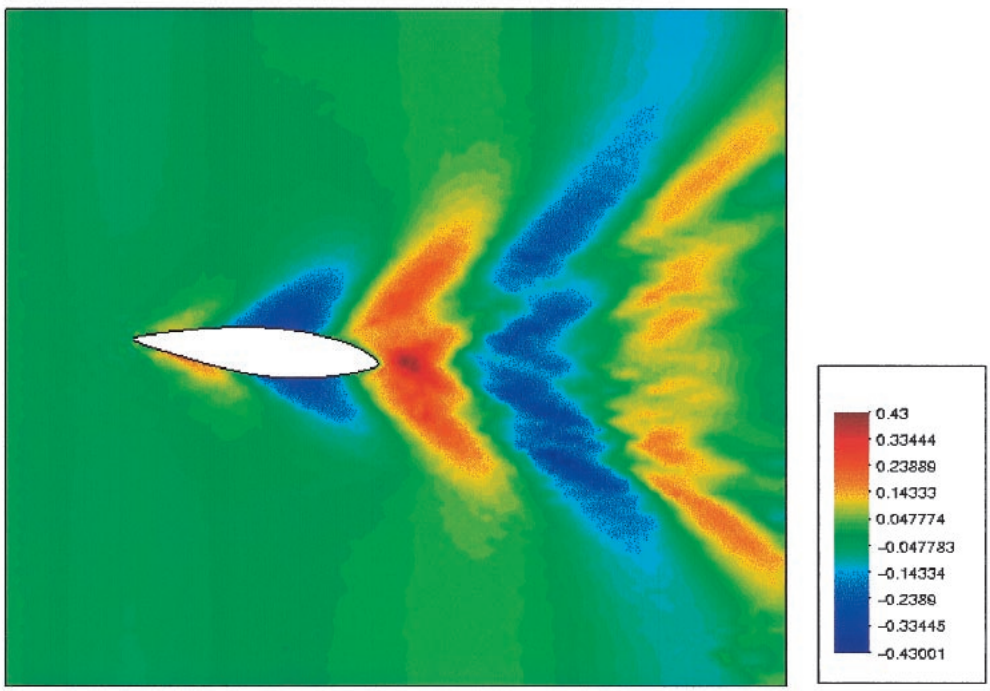

Plate 5. Sailing boat. Wave pattern at 10 knots

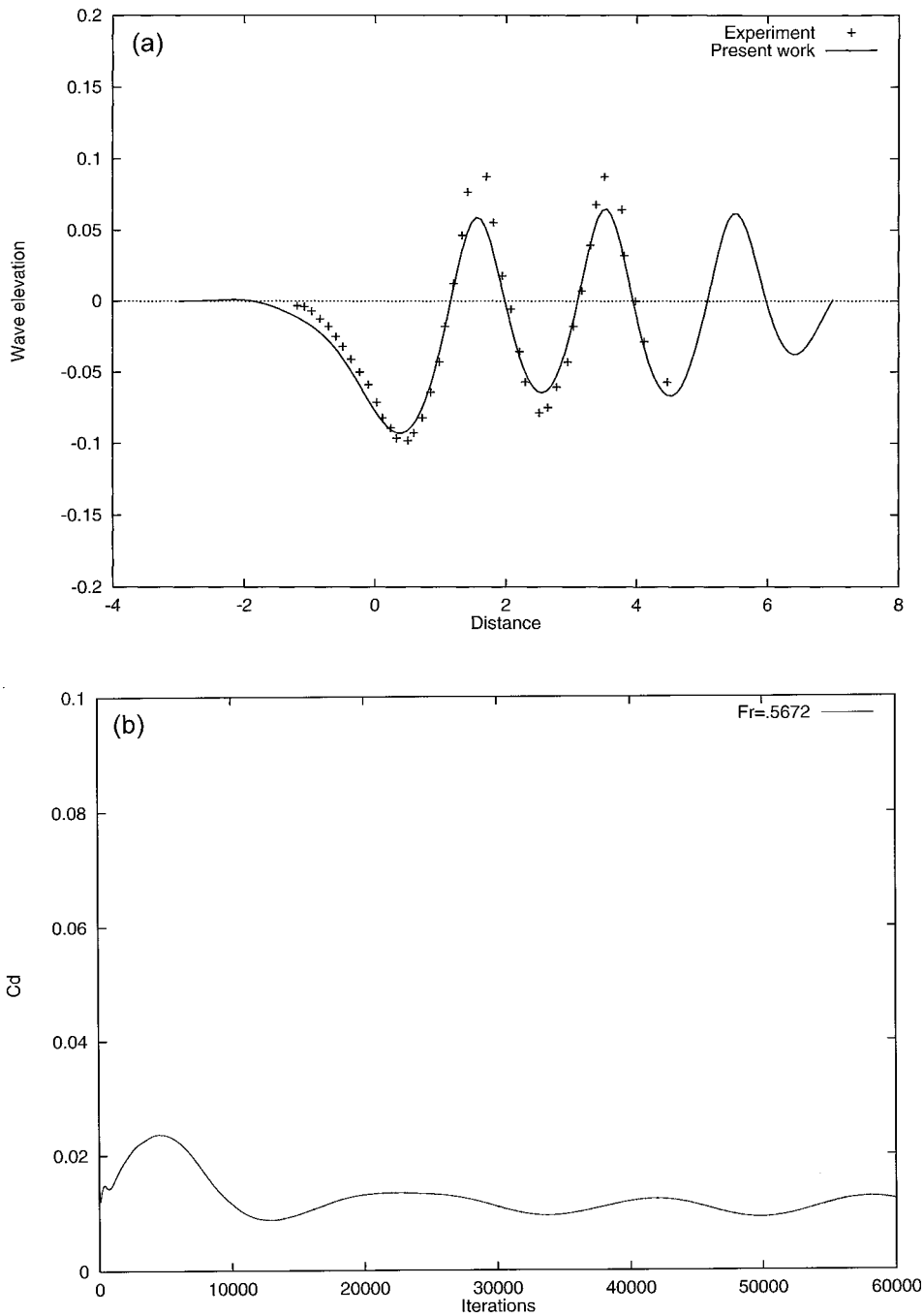

Figure 5. Submerged NACA0012: (a) Comparison of wave profiles; (b) Euler drag convergence history

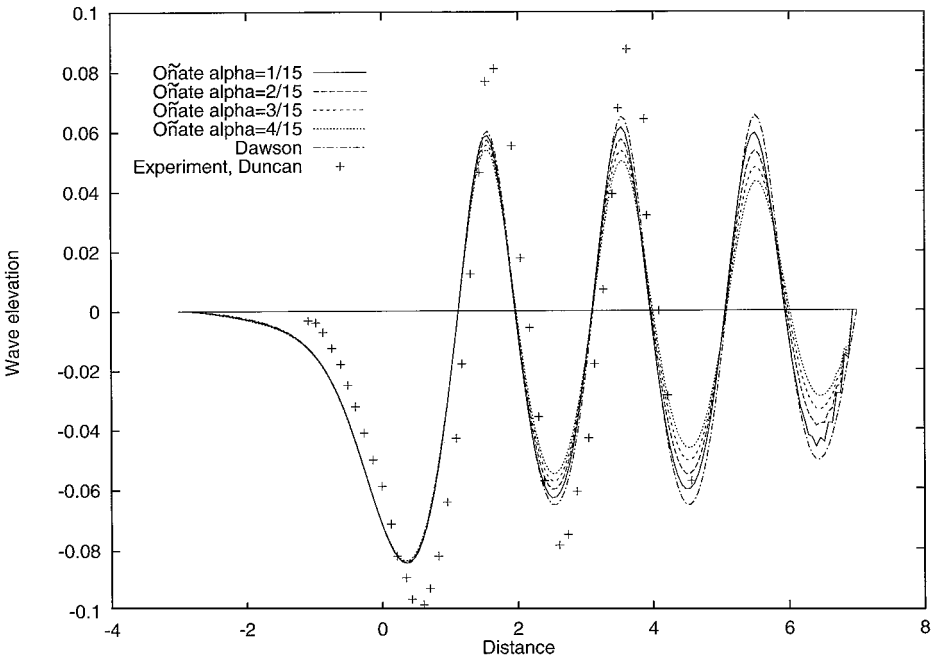

Figure 6. Submerged NACA0012. Comparison of wave profiles for different stabilizing formulae

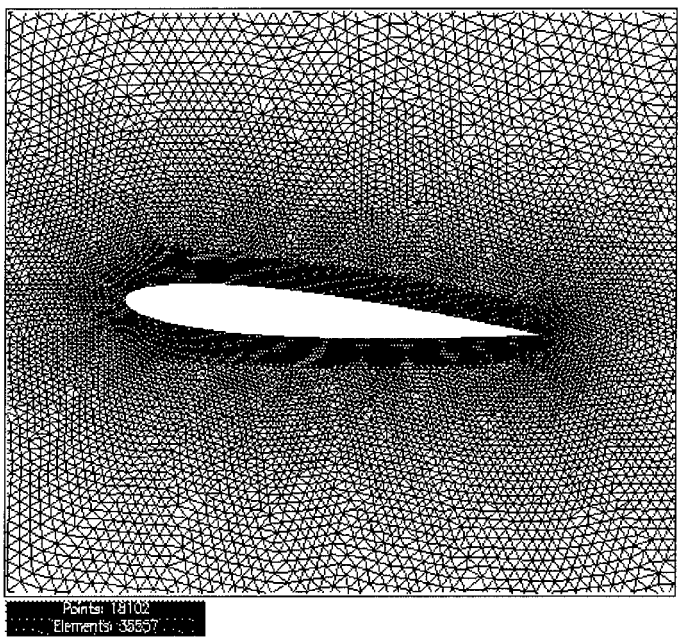

Figure 7. Submerged NACA0012. FE mesh for the Navier–Stokes solutions

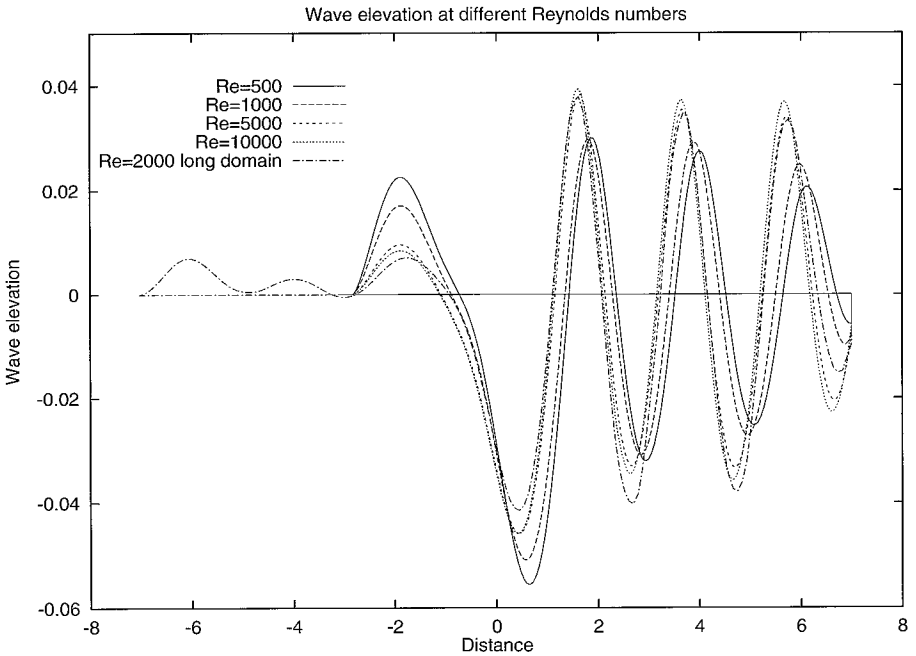

Figure 8. Submerged NACA0012. Waves profiles for different Reynolds numbers

8.2. *Wigley hull*

The first 3-D case considered here is the well-known Wigley hull, given by the analytical formula $y = 0{\cdot}5B(1-4x^2)(1-z^2/D^2)$ where B and D are the beam and the draft of the ship hull at still water.

The same configuration was tested experimentally in [50] and modelled numerically by several authors [40, 45]. We use here a non structured 3D finite element mesh of 65 434 linear tetrahedra, with a reference surface of 7800 triangles, partially represented in Figure 11. An inviscid Euler flow was considered with a variable velocity giving

$$Fr = \frac{\mathbf{u}}{\sqrt{gL}} = 0{\cdot}30, 0{\cdot}325, 0{\cdot}350, 0{\cdot}40 \quad \text{and} \quad 0{\cdot}45$$

Plate 3(a)–3(e) shows the surface patterns for different Froude numbers and Figure 12 shows the steady-state drag coefficient compared with experimental values. The drag coefficient is defined as

$$C_{\mathrm{d}} = \frac{\mathbf{F}_x}{(250/\pi)\rho\Omega\ \mathbf{u}_0^2}$$

where F_x is the resultant of the pressure forces in the x direction, ρ the density and Ω the equivalent surface defined as a function of the submerged volume V by

$$\Omega = V^{2/3}$$

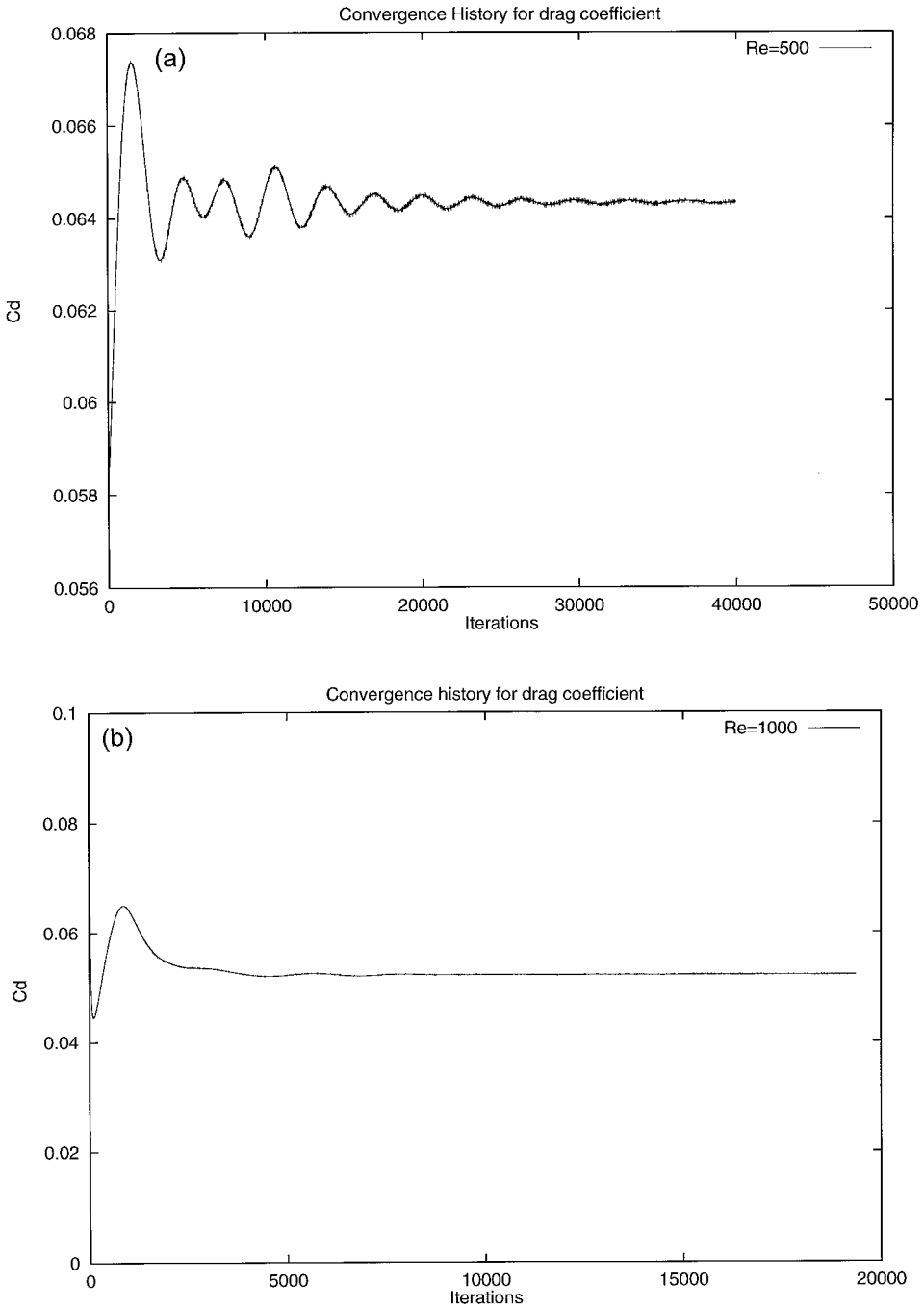

Figure 9. Submerged NACA0012. Convergence history for the drag coefficient: (a) $Re = 500$; (b) $Re = 1000$; (c) $Re = 5000$; (d) $Re = 10\,000$

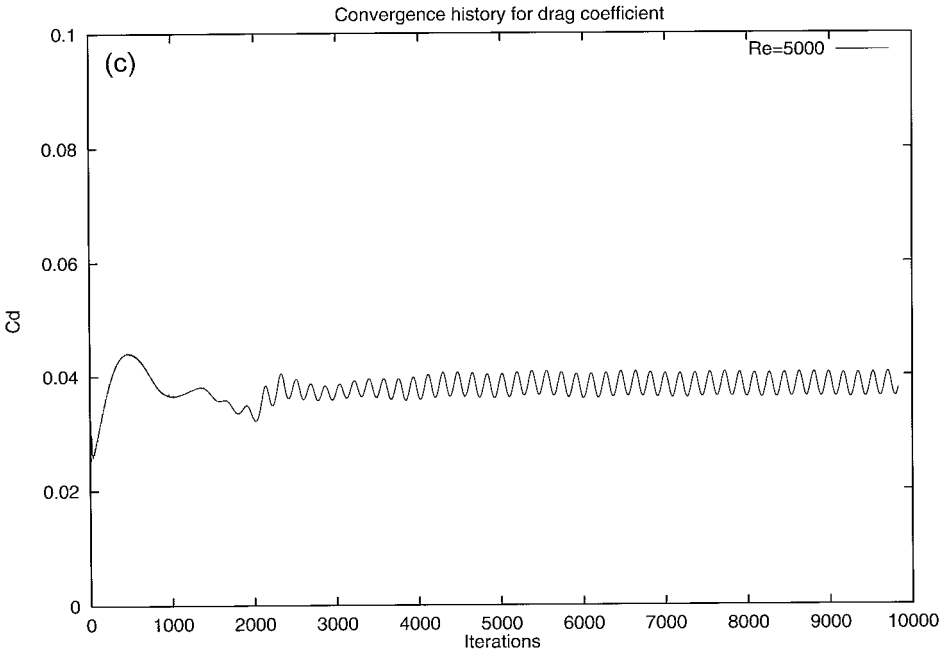

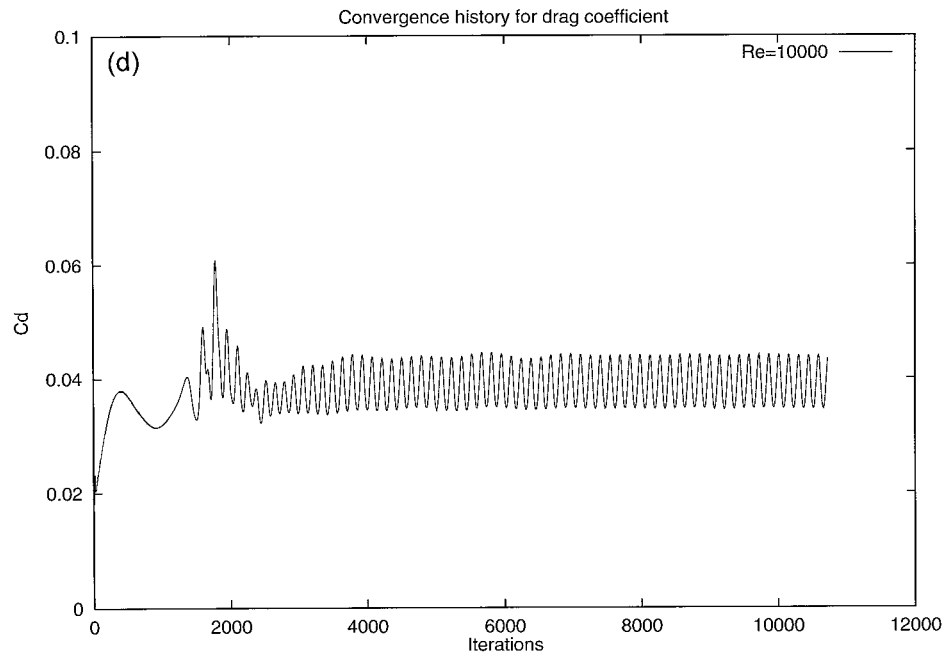

Figure 9. (*Continued*)

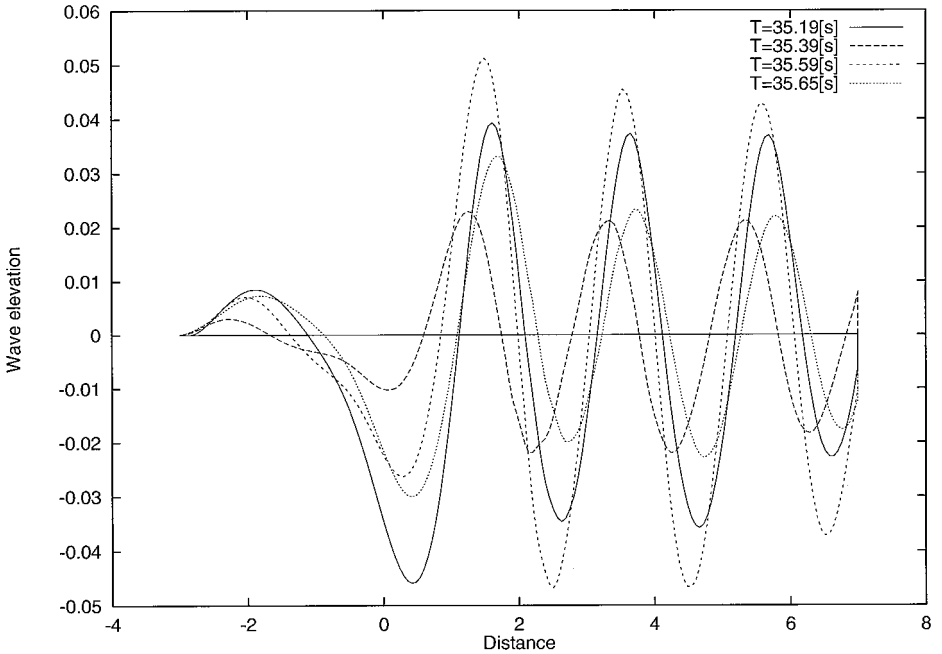

Figure 10. Submerged NACA0012. Wave elevation at $Re = 10\,000$ at different time steps

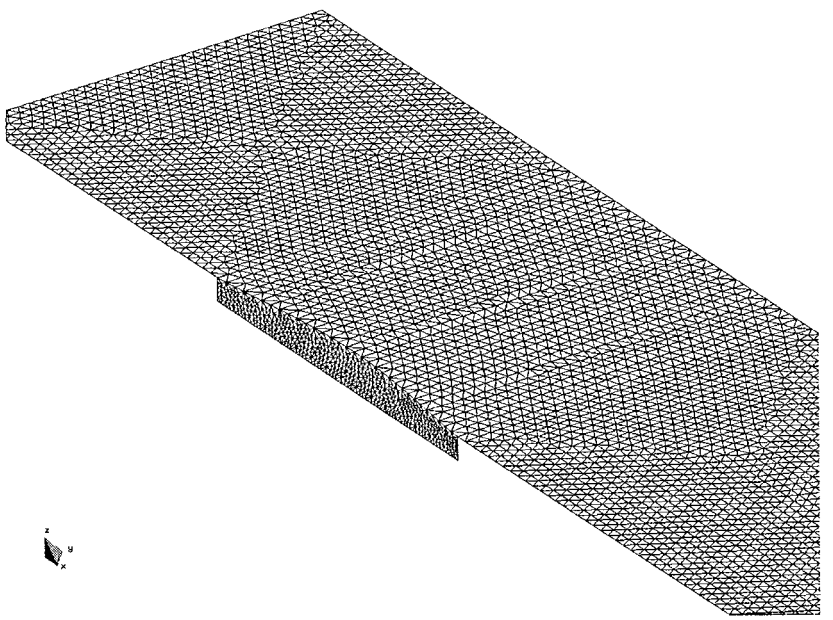

Figure 11. Wigley hull. Reference surface and hull mesh

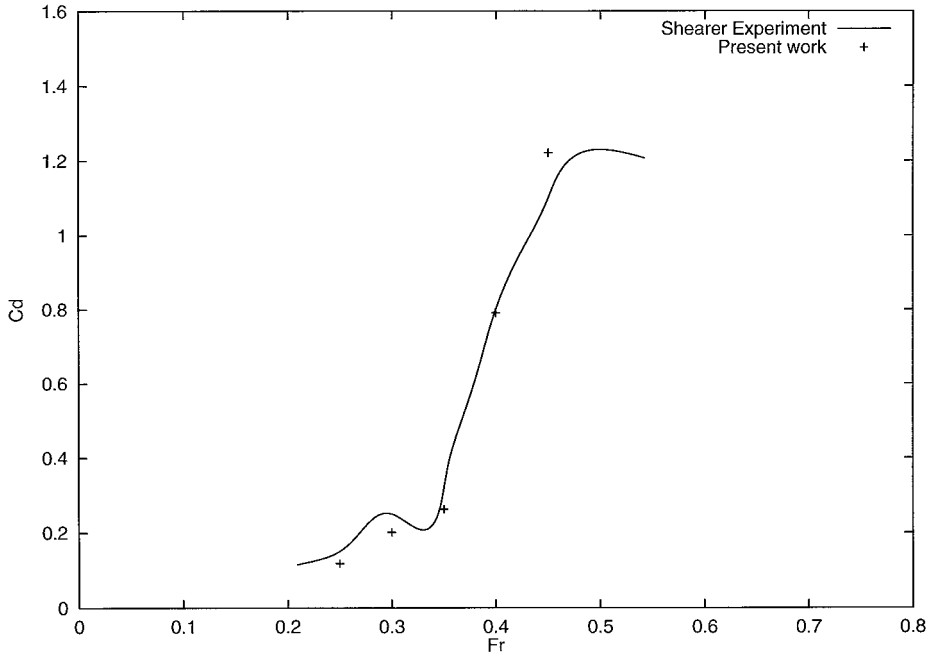

Figure 12. Wigley hull. Drag coefficient for differents Froude numbers

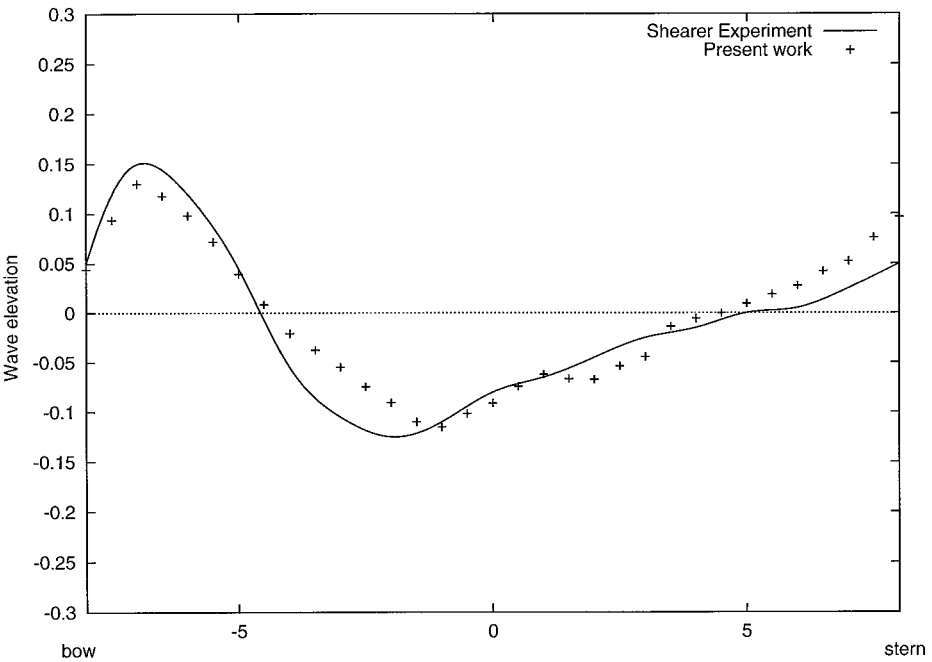

Figure 13. Wigley hull. Comparison of wave profile

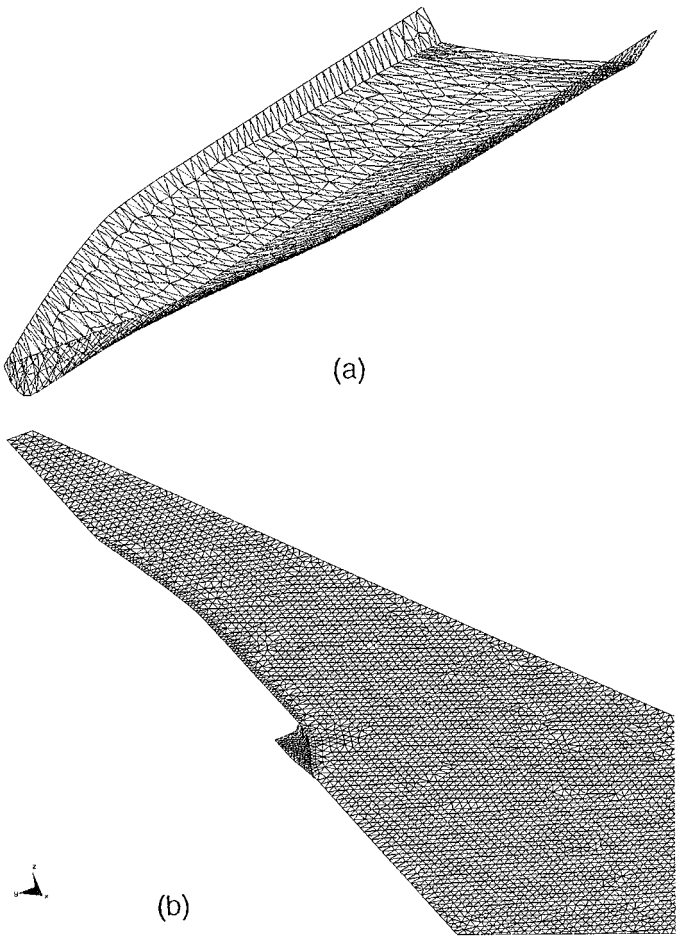

Figure 14. Fast ferry hull. Reference surface and hull mesh

Figure 13 represents the wave profile on the hull for $Fr = 0{\cdot}325$ which shows a good agreement with experimental values.

The time step used was the critical one and a total of 3000 time iterations were needed to obtain a stationary result. The stabilization scheme used was that given by equation (31) and $\Delta t^* = \Delta t$ was chosen for the integration of the free-surface.

Equation (43c) was solved using a conjugate gradient method with a total of 300 iterations during the first step and an average of 50 iterations in the rest.

8.3. Fast ferry ship hull

The third problem considered is a 3-D light weight fast ferry hull. The particular feature of this model is that it presents a transom stern producing a separation of the flow which introduces several difficulties in the free surface solution. The initial non-wave solution is too far from the

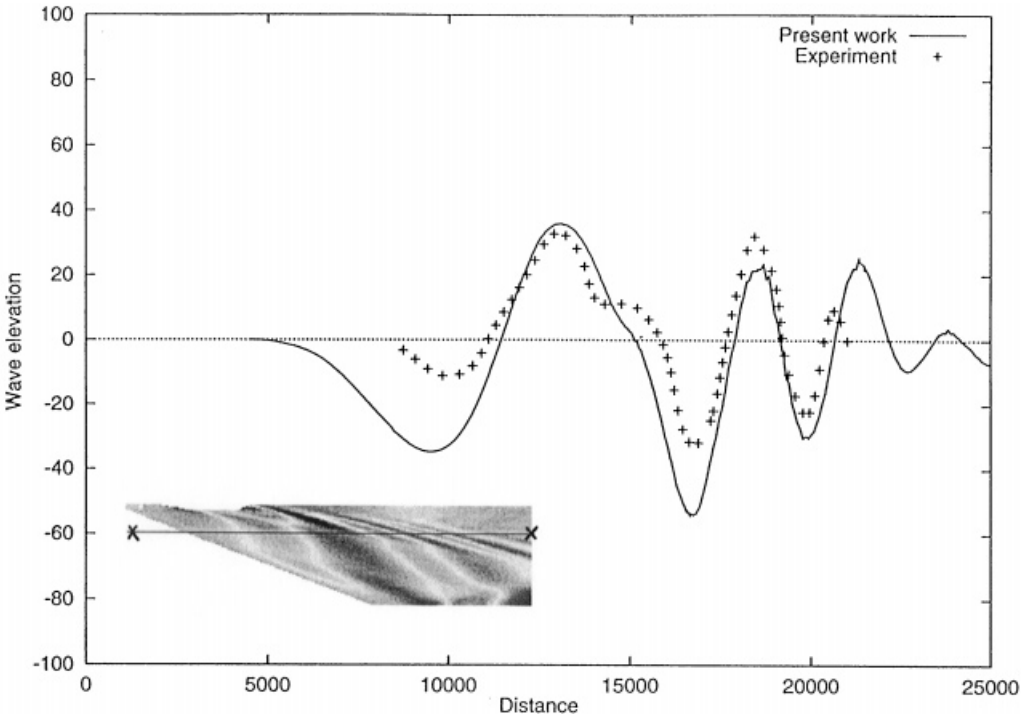

Figure 15. Fast ferry hull. Comparison of wave profile

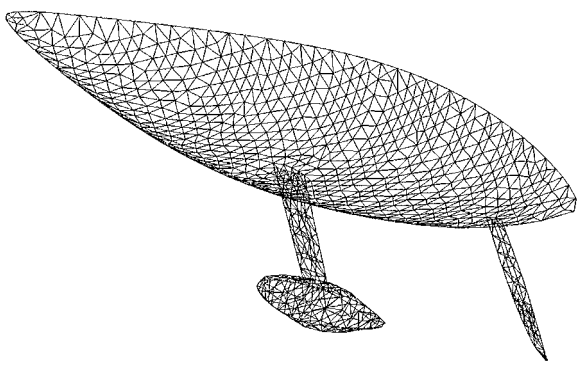

Figure 16. Sailing boat. Hull, keel, bulb and helm mesh

final free surface position and the flow pattern without waves is completely different near the stern from the final flow. In order to avoid this difficulty a $z \neq 0$ reference surface was defined in the vicinity of the stern where the free surface is expected. Figure 14 shows the mesh on the ship and the reference surface with the $z \neq 0$ part. A total of 197 853 linear tetrahedra with 27 357 triangles on the reference surface were used to solve the inviscid Euler case at a Froude number of 0·628 which is equivalent to 40 knots at full scale. A 1 : 25 scaled model was studied in order to compare with experimental results available. The non-dimensional wave drag resistance was

equal to $R_w = 0{\cdot}00149$ which was in agreement with the experimental value. Plate 4 shows the wave pattern obtained. The wave profile at a section of 2000 milimeter from the ship centreplane (50 m on the real ship) is displayed in Figure 15 where the experimental results have also been plotted. Note the good agreement between numerical and experimental values.

8.4. Sailing boat

The last example considered here is a sailing boat similar to those built for the America's Cup Sailing Competition. The sailing has a 25° heef angle and a drift angle of 4°. This is one of the cases in which the use of the Euler (or Navier–Stokes) equations instead of the potential flow equations is needed due to the difficulty of the potential model to satisfy correctly the Kutta–Joukoski condition on the trailing edge of the keel and helm.

Figure 16 shows a part of the mesh for the boat and the reference surface. A total of 104 577 linear tetrahedra were used in the volume mesh containing 14 010 triangles on the reference surface.

Due to the particular rounded shape of the stern and the fact that the hull shape presents a small angle with respect to the horizontal surface, a special treatment of this part was necessary. First of all, the local co-ordinate system (ξ, η), was defined using the streamlines obtained in the wave-free solution. Secondly, all the points belonging to the intersection between the stern with the reference surface were not considered as a free-surface. This simply implies that in those points the external pressure $\bar{p}$ is imposed when solving equation (43c).

Plate 5 shows the wave profile for a Froude number corresponding to a true sailing speed of 10 knots.

9. CONCLUSIONS

A methodology to solve the free-surface ship wave problem has been presented. The main features of the approach proposed are:

(1) Non structured finite elements mesh may be used.
(2) The non-linear free-surface boundary condition is introduced via an arbitrary reference surface which allows to move the free-surface while keeping the mesh fixed.
(3) The flow problem is solved with a semi-explicit fractional step method requiring only the implicit solution for the pressure. An iterative conjugate gradient algorithm has shown to be very efficient for solving this symmetric problem on small computers.
(4) The upwinding stabilization scheme proposed by Dawson has been generalized to non structured meshes with a more mathematically based explanation.
(5) A more suitable centred scheme has been proposed for evaluating the stabilization terms in the free-surface equation.
(6) The methodology may be applied to both Euler and Navier–Stokes incompressible flows, thus avoiding the difficulties of the Kutta–Joukoski condition.

ACKNOWLEDGEMENTS

Thanks are given to Mr. J. García for many useful discussions. The authors are also grateful to Mr. C. Morton and Ms. E. Mosso for their help in preparing the data for the analysis of the fast

ferry and the sailing boat examples. Thanks are also given to Mr. R. Darekar for his help in the analysis of the NACA profile.

The geometrical data and the experimental results for the fast ferry example were provided by the Spanish shipbuilder E.N. BAZAN, S.A. whose support and advice throughout this research is gratefully acknowledged. Thanks are also given to Copa America Desafio Español S.A. (CADESA) for providing the geometry of the sailing boat analysed.

REFERENCES

1. Raven H. A solution method for the non-linear ship resistance problem. *Doctoral Thesis*, Maritime Research Institute, The Netherlands, 1996.
2. Wehausen JV. The wave resistance of ships. *Advances in Applied Mechanics*, 1970.
3. Bai KJ, McCarthy JH, editors. *Proceedings of the Workshop on Ship Wave-Resistance Computations*. Bethesda, MD, USA, 1979.
4. Noblesse F, McCarthy JH, editors. *Proceedings of the Second DTNSRDC Workshop on Ship Wave-Resistance Computations*. Bethesda, MD, USA, 1983.
5. Dawson, CW. A practical computer method for solving ship-wave problems. *Proceedings of the 2nd International Conference on Numerical Ship Hydrodynamics*. USA, 1977.
6. Xia F. Numerical calculation of ship flows with special emphasis on the free-surface potential flow. *Ph.D. Thesis*, Chalmers University of Technology, Sweden, 1986.
7. Jenson G, Soding H. Ship wave resistance computation. *Finite Approximations in Fluid Mechanics* II 1989;**25**.
8. Kim YH, Lucas T. Nonlinear ship waves. *Proceedings of the 18th Symposium on Naval Hydrodynamics*. MI, USA, 1990.
9. D'Elia J, Storti M, Idelsohn S. A panel code for 3D wave drag calculations. *Report Grupo de Tecnología Mecánica del INTEC*, Güemes 3450, 3000 - Santa Fe, Argentina, 1995.
10. Reed AM, Telste JG, Scragg CA, Liepmann D. Analysis of transon stern flows. *Proceedings of the 17th Symposium on Naval Hydrodynamics*. The Hague, The Netherlands, 1990.
11. Nakos DE, Sclavounos Pd. On steady and unsteady ship wave patterns. *Journal of Fluid Mechanics* 1990;**215**: 256–288.
12. Raven H. A practical non-linear method for calculating ship wavemaking and wave resistance. *Proceedings of the 19th Symposium on Naval Hydrodynamics*. Seoul, Korea, 1992.
13. Beck RF, Cao Y, Lee TH. Fully non-linear water wave computations using the desingularized method. *Proceedings of the 6th Symposium on Num. Ship Hydrodynamics*. Iowa City, Iowa, USA, 1993.
14. Soding H. Advances in panel methods. *Proceedings of the 21th Symposium on Naval Hydrodynamics*. Trondheim, Norway, 1996.
15. Janson C, Larsson L. A method for the optimization of ship hulls from a resistance point of view. *Proceedings of the 21st Symposium on Naval Hydrodynamics*. Trondheim, Norway, 1996.
16. Mei CC, Chen HS, A hybrid element method for steady linearized free-surface flows. *International Journal for Numerical Methods in Engineering* 1976;**10**:1153–1175.
17. Bai KJ. A localized finite element method for steady, three-dimensional free-surface flow problems. Internal Report, David Taylor Naval Ship Research and Development Center, Bethesda, MD, 1979.
18. Chorin AJ. Numerical solution of the Navier–Stokes equations. *Mathematics of Computation* 1968;**22**:745–762.
19. Kim J, Moin P. Application of a fractional-step method to incompressible Navier–Stokes equations. *Journal of Computational Physics* 1985;**59**:308–323.
20. Hino T. Computation of free surface flow around and advancing ship by the Navier–Stokes equations. *Proceedings of the 5th International Conference on Num. Ship Hydrodynamics*. Hiroshima, Japan, 1989: 103–117.
21. Luo H, Baum JD, Löhner R. A finite volume scheme for hydrodynamic free boundary problems on unstructured grids. *AIAA*-95-0668, 1995.
22. Alessandrini B, Delhommeau G. A multigrid velocity-pressure-free surface elevation fully coupled solver for calculation of turbulent incompressible flow around a hull. *Proceedings of the 21st Symposium on Naval Hydrodynamics*. Trondheim, Norway, 1996:40–55.
23. Miyata H. Time-marching CFD simulation for moving boundary problems. *Proceedings of the 21st Symposium on Naval Hydrodynamics*. Trondheim, Norway, 1996:1–21.
24. Vazquez M, Codina R, Zienkiewicz OC. A fractional step method for the solution of Navier–Stokes equation. CIMNE Publication No. 103, 1996.
25. Chorin AJ. A numerical solution for solving incompressible viscous flow problems. *Journal of Computational Physics* 1967;**2**:12–26.
26. Rizzi A, Erikson L. Computation of inviscid incompressible flow with rotation. *Journal of Fluid Mechanics* 1985; **153**:275–312.

27. Farmer JR, Martinelli L, Jameson A. A fast multigrid method for solving incompressible hydrodynamic problems with free surfaces. *AIAA Journal* 1993;**32**(6):1175–1182.
28. Peraire J, Morgan K, Peiro J. The simulation of 3D incompressible flows using unstructured grids, In: Caughey DA, Hafez MM, editors. *Frontiers of Computational Fluid Dynamics*; Wiley: New York, 1994, Chapter 16.
29. Briley WR, Neerarambam SS, Whitfield DL. Multigrid algorithm for three-dimensional incompressible high-Reynolds number turbulent flows. *AIAA Journal* 1995;**33**(1):2073–2079.
30. Sheng C, Taylor LK, Whitfield DL. Implicit lower-upper/approximate-factorization schemes for incompressible flows. *Journal of Computational Physics* 1996;**128**(1):32–42.
31. Storti M, Nigro N, Idelsohn SR. Steady state incompressible flows using explicit schemes with an optimal local preconditioning. *Computer Methods in Applied Mechanics and Engineering* 1995;**124**:231–252.
32. Idelsohn SR, Storti M, Nigro N. Stability analysis of mixed finite element formulation with special mention to stabilized equal-order interpolations. *International Journal for Numerical Methods in Fluids* 1995;**20**:1003–1022.
33. Baba E, Takekuma K. A study on free-surface flow around bow of slowly moving full forms. *Journal of the Society of Naval Architects Japan* 1975;**137**.
34. Newman JN. Linearized wave resistance theory. *International Seminar on Wave Resistance*. Tokyo/Osaka, *Journal of the Society of Naval Architects Japan*, 1976.
35. Eggers K. Non-Kelvin dispersive waves around non-slender ships. Schiffstechnik, Bd. 28, 1981.
36. Eggers K. On the dispersion relation and exponential amplitude variation of wave components satisfying the slow ship differential equation on the undisturbed free-surface. In: Inui T, editor. *Study on Local Non-Linear Effect in Ship Waves*, Tokyo, 1980.
37. Brandsma FJ, Hermans AJ. A quasi-linear free-surface condition in slow ship theory. Schiffstechnik, Bd. 32, 1985.
38. Nakos DE. Ship wave patterns and motions by a three-dimensional Rankine panel method. *Ph.D. Thesis*, MIT, Cambridge, MA, USA, 1990.
39. Baba E, Hara M. Numerical evaluation of a wave-resistante theory for slow ships, *2nd International Conference on Numerical Ship Hydrodynamics*. Berkeley, USA, 1977.
40. Löhner R, Yang C, Oñate E, Idelsohn S. An unstructured grid-based parallel free-surface solver. *Report CIMNE No.* 99 Barcelona, 1996.
41. Codina R. On stabilized finite element method for linear systems of convection-diffusion reaction equations. *Research Report PI 126*, CIMNE, Barcelona, 1997.
42. Oñate E. On the stabilization of numerical solution for advective–diffusive transport and fluid flow problems. *Research Report No.* 81, CIMNE, Barcelona, 1996. *Computer Methods in Applied Mechanics and Engineering* 1998;**151**:1–2, 233–267.
43. Oñate E, García J, Idelsohn S. Computation of stabilization parameter for the finite element solution of advective–diffusive problems. *International Journal for Numerical Methods in Fluids* 1997;**25**:1385–1407.
44. Oñate E, Idelsohn S. Stabilization of the numerical solutions for the free surface wave equation in fluid dynamics. Published In: Papailiou K *et al.*, editors, ECCOMAS98; Wiley: New York, 1998.
45. Hino T, Martinelli L, Jameson A. A finite volument method with unstructured grid for free-surface flow. *Proceedings of the 6th International Conference on Num. Ship Hydrodynamics*. Iowa City, IA, 1993:173–194.
46. Zienkiewicz OC, Codina R. A general algorithm for compressible and incompressible flow. Part I: the split characteristic based scheme. *International Journal for Numerical Methods in Fluids* 1995;**20**:869–85.
47. Zienkiewicz OC, Morgan K, Satya Sai BVK, Codina R, Vázquez M. A general algorithm for compressible and incompressible flow. Part II: tests on the explicit form. *International Journal for Numerical Methods in Fluids* 1995;**20**(8–9):886–913.
48. Zienkiewicz OC, Taylor RL. *The Finite Element Method*, vol. II.; McGraw-Hill: New York, 1989.
49. Duncan JH. The breaking and non-breaking wave resistance of a two-dimensional hydrofoil. *Journal of Fluid Mechanics* 1983;**126**.
50. Cooperative Experiments on Wigley Parabolic Models in Japan. *17th ITTC Resistance Committee*, *Report*, 2nd ed., 1983.
51. Chen HS, Mei CC. Calculations of two-dimensional ship waves by a hybrid element method based on variational principles. *Proceedings of 1st International Conference on Num. Ship Hydrodynamics*. Sponsored by David Taylor Naval Ship Research and Development Center: Bethesda, 1975;95–111.
52. Bai KJ. A localized finite element method for the uniform flow problem with a free-surface. *Proceedings of 1st International Conference on Num. Ship Hydrodynamics*, Sponsored by David Taylor Naval Ship Research and Development Center: Bethesda, MD, 1975.
53. Darekar R, Sacco C, Idelsohn S, Oñate E. Solution of Navier–Stokes equations with the free surface boundary conditions using unstructured finite element grids. *Research Report No.* 116, CIMNE, Barcelona, 1997.

